Combustion and Flame 266 (2024) 113533

Contents lists available at ScienceDirect

Combustion and Flame

journal homepage: www.sciencedirect.com/journal/combustion-and-flame

Relative reactivity of methyl anisole isomers: An experimental and kinetic modelling study

Karl Alexander Heufer [a,*], Rene Daniel Büttgen [a], Luna Pratali Maffei [b], Matteo Pelucchi [b]

[a] Chair of High Pressure Gas Dynamics, Shock Wave Laboratory, RWTH Aachen University, Aachen 52056, Germany
[b] CRECK Modelling Lab, Department of Chemistry, Materials and Chemical Engineering "G. Natta", Politecnico di Milano, P.zza Leonardo da Vinci 32, 20133 Milano, Italy

ARTICLE INFO

Keywords:
Methyl-anisole
Shock tube
Rapid compression machine
Detailed kinetic model

ABSTRACT

Due to the current interest in biomass derived carbon neutral fuels and fuel additives for gasoline engines and to the growing need of understanding the fundamentals of gas phase combustion in the context of wildfires, this study investigates the combustion behavior of key components of biomass pyrolysis oils, namely the three methylanisole isomers (ortho-, meta- and para-methylanisole). Specifically, this study presents the first experimental ignition delay time measurements for such fuels using a shock tube and a rapid compression machine. Ignition experiments were carried out for stoichiometric fuel/air mixtures ($\varphi = 1$) at compressed pressure $p_c = 10$ and 20 bar, covering a temperature range $T_c = 880$–1220 K. A kinetic model based on previous efforts in the area of oxygenated aromatic hydrocarbon fuels is proposed to reproduce and interpret the experimental findings, specifically focusing on capturing the observed different reactivity of the three isomers. To this aim, thermodynamic properties of primary intermediates and bond dissociation energies were calculated highlighting relevant differences originated from the relative position of the O–CH_3 and –CH_3 substituents. In addition, an isomerization pathway specific to the ortho isomer was theoretically investigated and found to motivate the observed higher reactivity with respect to the meta and para isomers

Novelty and significance statement

In context of the need for sustainable fuels in the transport sector but also in regards to wildfires, understanding the combustion behaviour of lignin reference structures is of fundamental interest. This study focuses on the influence of structural configuration in poly-substituted oxygenated aromatics by investigating the oxidation kinetics of the three methyl-anisole isomers. For the first time experimental ignition delay time measurements for such fuels using a shock tube and a rapid compression machine are presented. Furthermore, a novel kinetic sub-mechanism is developed which is capable of predicting the significant difference in reactivity of 2-methyl-anisole versus 3- and 4-methylaniosle. Model analysis revealed that reaction pathways unique for 2-methyl-anisole are the main drivers for the observed differences in the fuel's reactivity.

1. Introduction

Climate change mitigation measures and the decarbonization of the energy economy motivate a strong interest in the production of sustainable, carbon-neutral fuels for the transport sector [1]. Biomass conversion technologies, such as fast pyrolysis, are a viable option for the large-scale production of carbon-neutral fuels or fuel additives, as well as chemicals [2]. Lignin, one of the major components of lignocellulosic biomass, is a heterogeneous polymer composed of several aromatic monolignols carrying a variety of functional groups, mostly containing oxygen atoms such as hydroxy and methoxy groups. Lignin conversion with fast pyrolysis yields the so-called biomass-derived bio-oils which contain a large variety of oxygenated aromatic compounds, reflecting the complexity of the starting material [3]. Within these, non-substituted or mono-substituted aromatic compounds (e.g. benzene, toluene, phenol, anisole) have all been shown to have low reactivity and could potentially be used as anti-knock additives [4,5]. In contrast, the behavior of poly-substituted oxygenated aromatics may either increase or decrease the fuel knocking potential depending on the

* Corresponding author.
E-mail address: heufer@hgd.rwth-aachen.de (K.A. Heufer).

https://doi.org/10.1016/j.combustflame.2024.113533
Received 8 March 2024; Received in revised form 23 May 2024; Accepted 25 May 2024
Available online 7 June 2024

interaction between the side groups. For instance, guaiacol (i.e., an aromatic ring with hydroxyl and methoxy substituents in ortho position) has a derived cetane number (DCN) of 19.3 [6] and isooctane has a cetane number of less than 19 [7], and is therefore more prone to autoignition compared to isooctane. On the other hand, 4-methylanisole has a high Research Octane Number (RON) of 104 [6] and is therefore less likely to autoignite compared to isooctane.

Another motivation for studying lignin-derived oxygenated aromatic structures is to understand the fundamentals of gas-phase combustion in the context of wildfires. Wildfires are a critical threat to nature, people, and property and their occurrence is increasing in frequency and intensity [8]. A detailed investigation of the combustion behavior of representative compounds can provide the foundation for the development of more accurate lower-order models for wildfire simulation.

Despite the widespread interest in the reactivity of oxygenated aromatic hydrocarbons, the availability of accurate rate constants for their decomposition and oxidation processes is still scarce. Therefore, research efforts in recent years have focused on highly accurate theoretical calculations to determine both the reactivity of mono-substituted aromatic hydrocarbons (MAHs) and the effect of multiple substituents on the aromatic ring. In particular, we investigated theoretically the most important reactions in phenol decomposition [9], as the representative of hydroxy-substituted aromatics. Then, we performed systematic theoretical investigations of H-atom abstraction reactions from a set of mono-substituted MAHs [10]. Finally, we evaluated the effects of the presence of multiple substituents through the estimation of bond dissociation energies (BDEs), the identification of peculiar reaction classes [11], and the systematic theoretical investigation of H ipso substitution reactions on a variety of mono and di-substituted MAHs [12], leading to the determination of rate rules for this reaction class. In the latter study, it was verified that for mono-substituted oxygenated aromatic hydrocarbons (mono-substituted OAHCs) only the nature of the substituents influences the overall reactivity, whereas for poly-substituted oxygenated aromatic hydrocarbons (poly-substituted OAHCs), also the relative position of the side groups affects the overall reactivity. Such influence can be substantial for some reaction classes such as oxygen recombination for alkylated aromatics and radical decomposition or oxidation for oxygenated aromatics, as confirmed by several experimental studies [13–15].

Despite our theoretical efforts, only few experimental assessments using multiple isomers of a given OAHC with multiple substitutions were able to confirm our findings [15,16], resulting in a knowledge gap between theoretically determined evidence of proximity effects and their actual impact on OAHC fuels reactivity. To fully exploit the potential of biomass-derived bio-fuels and fuel additives that drives bio-oil upgrading processes toward a certain distribution of functional group for use in spark ignition engines, this knowledge gap needs to be filled by a systematic experimental characterization of the reactivity of different isomers carrying the same functionalities.

This work represents an important step in this direction. Indeed, an experimental, theoretical and modeling investigation of the isomers of methylanisole (MA), for which, to date, no dedicated combustion related experimental or kinetic modelling works are reported in the literature, is presented. Specifically, we investigate the autoignition behavior of the three MA isomers, namely 2MA, 3MA and 4MA (o-, m-, p-methylanisole or o-, m-, p-$CH_3C_6H_4OCH_3$, respectively). The latter was found in significant amounts in biomass pyrolysis oils and was highlighted as a possible promising candidate as a drop-in fuel component for gasoline [5]. To the authors' knowledge, no experimental data have been reported on the oxidation and combustion behavior of three fuels concerning. Experimental ignition delay times are measured here using a high-pressure shock tube (ST) and a rapid compression machine (RCM) ultimately aiming to characterize the effect of different molecular structures on relative reactivities under engine-relevant conditions.

As highlighted in [11,15,17–19] the remarkably low BDE of the O–C bond in the methoxy substituents on aromatic hydrocarbons (i.e., 257–264 kJ/mol) has a strong influence on the overall reactivity of anisole, guaiacol and vanillin. Hence, in this work the BDEs of the corresponding O–C bonds in all three MA isomers are calculated. Theoretical calculations also include the hydrogen atom shift in 2MA radicals from the methoxy to the methyl groups $oCH_3C_6H_4O\dot{C}H_2 = o\dot{C}H_2C_6H_4OCH_3$, which turns out to be the relevant step in explaining the differences in MA isomers kinetic behavior.

Finally, a previously developed anisole model [19] is here updated to include MA pyrolysis and combustion kinetic subsets using established approaches based on reaction classes and rate rules [9,11,12]. The model developed in this way is used to simulate and interpret the results of the experimental measurements, focusing on the different reactivity of the MA isomers.

2. Experimental method

Ignition delay time (IDT) measurements of the three methylanisole isomers 2MA, 3MA and 4MA were performed in the HGD Rapid Compression Machine (RCM) and the HGD Shock Tube (ST) at RWTH Aachen University. The IDT is defined as the time delay between reaching a compressed state (due to a piston in the RCM, and a reflected shock wave in the ST) and the maximum pressure rise (max. dp/dt) due to auto-ignition. Two datasets (1 and 2 MPa, with varying compression temperature T_c) for each isomer in each facility were measured, resulting in 12 datasets, as summarized in Table 1. The three isomers were obtained from Merck with a purity of >99.5 %. Oxygen (≥ 99.999 %), nitrogen (≥ 99,999 %) and argon (≥ 99.999 %) were obtained from Westfalen AG.

2.1. Rapid compression machine (RCM)

The RCM consists of three main parts: the reaction chamber, the hydraulic section, and the pneumatic section and is described in detail in [20–22]. The reaction chamber has a 50 mm bore, and uses a single creviced piston configuration accelerated pneumatically in a single, linear stroke (250 mm displacement). The creviced piston of the reactor chamber ensures a homogeneous temperature in the core after the end of compression is reached, as described by Mittal et al. [23]. Variation of the conditions at end of compression was achieved by varying the initial pressures in the reactor and changing the compression ratio through an adjustable end wall. Initial temperature and diluent gas composition were kept constant throughout all experiments in this study.

Initial temperatures were monitored and feedback-controlled with several type T thermocouples and a 3-wire PT100 temperature sensor distributed over the reactor part of the RCM. In this study the reactor and the manifold of the RCM were pre-heated to 125 °C to prevent fuel condensation. The static pressure during mixture and experiment preparation was measured by two pressure sensors mounted in the manifold system (STS PTM/RS485; for up to 50 kPa and up to 0.5 MPa, respectively). The dynamic pressure during the reactive and non-reactive experiments was measured by a piezoelectric sensor (Kistler 6125CU20) in a recessed configuration as described by Ramalingam et al. [22]. All fuel-air mixtures were prepared in separate stainless steel mixing vessels and allowed to homogenize prior to the experiment. Taking into account all measurement uncertainties of the temperature and pressure sensors, uncertainties of ± 1 % in temperature and ± 0.5 % in pressure at the end of compression were calculated according to

Table 1
Overview of the experimental matrix for the three investigated fuels (2MA, 3MA, 4MA).

Facility	p_c MPa	ϕ –	Dilution –	Fuel mol%	O_2	Ar	N_2
RCM	1 & 2	1	3.762 ("in-air")	2.04	20.59	30.92	46.44
ST				2.04	20.59	0	77.36

Weber et al. [24].

For each experimental condition at least two reactive experiments were performed to ensure repeatability of the results. In addition, non-reactive experiments were performed to derive effective volume profiles that can describe the compression and heat loss characteristics of the RCM experiments in simulation. In these experiments, oxygen is replaced by nitrogen to suppress exothermic reactions. Further details on this method can be found in [25]. A representative pressure plot of a reactive experiment versus a non-reactive experiment is shown in Fig. 1.

2.2. Shock tube (ST)

A detailed description of the HGD high-pressure shock tube (ST) can be found in [26,27]. Briefly, the HGD ST has a 3 m long curved driver section, a 4.1 m long driven section, inner diameter of 63.5 mm and is designed for peak ignition pressures of up to 50 MPa. The driven section and the driver section are separated by a double diaphragm chamber. Similar to the RCM, the ST and its manifold were heated to 125 °C. Again, temperatures were monitored and feedback controlled by several type T thermocouples, placed on the tube and the manifold. Pressure levels in the system were monitored by two pressure sensors (STS ATM1st; for up to 50 kPa and up to 1.0 MPa, respectively) and mixtures were prepared in a stainless-steel mixing vessel.

The shock velocity was measured by five pressure transducers (PCB 113B22) placed in the driven section towards the end of the tube. Major uncertainties in the conditions behind the reflected shock arise from uncertainties in the measured shock velocities and are estimated to be 0.7 % in temperature and 1.5 % in pressure [27]. Further, shock attenuation might affect the conditions behind the reflected shock over time. Typically, however, pressure and temeperature rise induced by shock attenuation affects the ignition delay time only at longer measurement times, i.e., lower temperatures. Under these conditions an average pressure rise rate of 8 %/ms has been observed in experiments. To accurately determine this pressure gradient, the pressure sensor closest to the endwall (9 mm), which is also used to determine the ignition delay time, was shielded by a thin silicone layer to minimize heat shock affects [28]. Fig. 2 shows a representative pressure profile from a shock tube experiment.

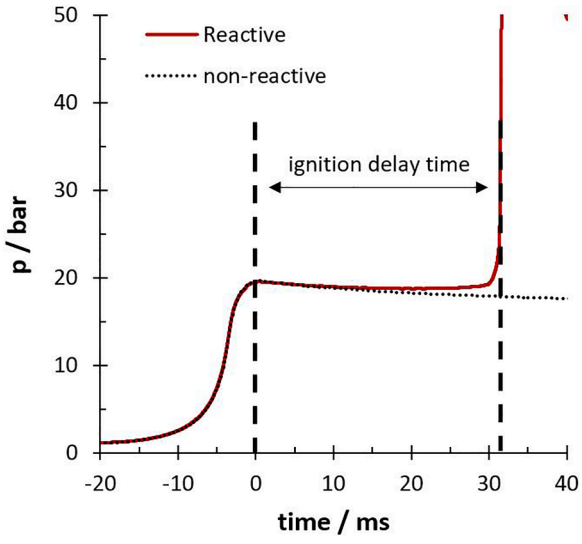

Fig. 1. Representative pressure profile in the RCM (Fuel: 2MA, φ = 1.0, T at end of compression: 837 K).

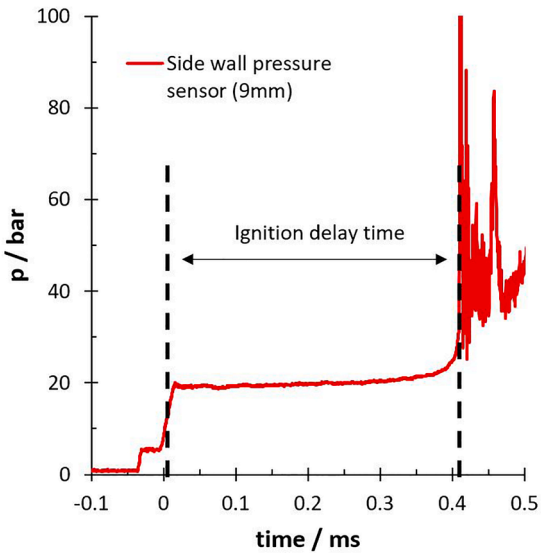

Fig. 2. Representative pressure profile in the ST (Fuel: 2MA, φ = 1.0, T behind reflected shock: 1036 K).

3. Theoretical calculations

3.1. Methodology

The theoretical calculations of this work primarily focused on determining the BDEs for all three MA isomers considered, first to allow for a macroscopic assessment of the expected impact on fuel reactivity of relative bond strengths. In particular, we determined the BDEs for the C–H bonds in the methyl and methoxy substituents, the O–CH_3 methoxy BDEs, and the C–OCH_3 BDEs and the C–CH_3 BDEs (where the first C indicates the carbon of the aromatic ring), for a total of 15 BDEs. As anticipated in the introduction, we also determined the rate constant for the isomerization between o$CH_3C_6H_4OCH_2$ and o$CH_2C_6H_4OCH_3$ radicals, which represent a key reaction in differentiating the reactivity of o$CH_3C_6H_4OCH_3$ with respect to the other isomers.

Theoretical calculations were performed using EStokTP [29], as extensively described in our previous works [9,10,12]. Gaussian G09 [30] was used for geometry optimization and frequency calculations, while Molpro 2019 [31] was used for single point energy calculations at the coupled cluster level. The isomerization rate constant was determined with Ab Initio Transition State Theory based Master Equation simulations (AI-TST-ME). The pressure-dependent rate constant for the H transfer reaction was computed with MESS [32] using the variational implementation of TST. Intrinsic reaction coordinate calculations were performed taking steps of 0.02 Å in the direction of both reactants and products. The geometries and the vibrational frequencies of the considered species and of the saddle point on the isomerization PES were computed with Density Functional Theory (DFT) using the ωB97X-D functional [33] and the 6-311+G(d,p) basis set, successfully adopted in our recent works on phenol and phenoxy decomposition [9] and ipso-substitution reactions on MAHs [12].

The single point energies were refined at the CCSD(T)/aug-cc-pVTZ level of theory [34], and corrected for basis set size dependence with the energy change between density fitted (DF)-MP2/aug-cc-pVQZ and DF-MP2/aug-cc-pVTZ [35]. The resulting values for the T1 diagnostics were satisfactorily below 0.02 for all species (see Table S3), hence no additional multireference calculations were deemed necessary.

Torsional motions were treated according to the one-dimensional hindered rotor approximation for the calculation of the partition functions. The rotation potential was computed scanning the torsional angle with 20° intervals, performing the electronic structure calculations at the same level of theory used for the geometry optimization. Finally,

tunneling effects were accounted for using the Eckart model [36].

Thermochemical properties of methylanisole isomers and the corresponding radicals were derived by post-processing the theoretical calculations using AutoMech suite of codes [37]. Additionally, the thermochemistry of $oCH_3C_6H_4OCH_2O\dot{O}$ was computed due to its relevance in the equilibrium of the oxygen addition to the radical of 2MA ($R + \dot{O}_2 <=> R\dot{O}_2$), which was discovered during model development. Due to the larger system size, in this case electronic energies were computed at the FNO-CCSD(T)/cc-pVQZ level of theory and extrapolated to the complete basis set using the scaling $0.69399\cdot(E_{QZ} - E_{TZ})$ [35], where E_{QZ} and E_{TZ} indicate the electronic energies computed using cc-pVQZ and cc-pVTZ basis sets, respectively. Formation enthalpies of the species of interest were computed using, where possible, isodesmic reaction schemes. In particular, reference species considered were $C_6H_5OCH_3$, $C_6H_5CH_3$, C_6H_6, $C_6H_5\dot{O}$, C_6H_5, $C_6H_5\dot{C}H_2$, $CH_3O\dot{C}H_2$, CH_3OCH_3. The 0 K formation enthalpies thus derived as well as those computed from different reaction schemes are reported for comparison in Table S4. Reference formation enthalpies were taken from the Active Thermochemical Tables (ATcT) [38]. Due to the lack of experimental data for the thermochemistry of the species considered, we considered anisole as a reference species to provide a rough uncertainty estimate of the present calculations. The same reaction schemes applied to derive the formation enthalpy of anisole [39] resulted in less than 0.8 kJ/mol difference with respect to ATcT recommended values at both 0 K and 298 K. However, the heat capacity derived from theoretical calculations underestimates the experimental values of Hales et al. [40] by about 6 – 8 J/mol/K in the 400 – 500 K range (see Table S5). Such discrepancies might result in larger deviations in the high-temperature formation enthalpies (i.e., about 4 kJ/mol around 1000 K and about 9 kJ/mol at 2000 K), which are however expected to partially compensate in the calculation of chemical equilibria considering that the same theoretical methodology was adopted for the derivation of thermochemical properties for the main radicals. Assuming that a similar discrepancy applies to methylanisole isomers, an uncertainty below 2 kJ/mol is expected for the 0 K formation enthalpy of molecules, while higher differences may be found for radicals as well as for higher temperature values. Finally, the uncertainty in the formation enthalpy of the peroxy radical $oCH_3C_6H_4OCH_2O\dot{O}$ is expected to be larger since no appropriate connectivity-based hierarchy (CBH) scheme was found for the calculations with the available reference species of ATcT database. Hence, its formation enthalpy is computed directly from the calculated reaction energy of the oxygen addition to o-$CH_3C_6H_4O\dot{C}H_2$ radical. Overall, BDEs of all MA isomers were computed with two different methods, i.e., 1) from the calculated reaction enthalpies of the corresponding bond-fission reactions (referred to as directly calculated "direct"), 2) from the 0 K formation enthalpies obtained as above (referred to as pseudo-experimental "pseudo"). The differences between these two methods allow a more accurate estimate of the uncertainties that will be discussed in the results (Section 3.2).

The rate constant of the isomerization reaction was computed in the 300–2000 K temperature and 0.1–100 atm pressure ranges. The collisional energy transfer probability is described using the exponential down model [41]. Collisional and energy transfer parameters were adopted from a recent work on toluene oxidation reactivity [42]. The computed rate constant was fitted according to the modified Arrhenius expression.

3.2. Calculation results

3.2.1. Bond dissociation energies

The calculated BDEs from this study are reported in Table 2. Overall, it is evident that the O–CH_3 BDE has the lowest BDE by far, as expected. Due to the low bond strength the decomposition involving the O–CH_3 bond cleavage has a strong influence even at low temperatures as

Table 2
Bond dissociation energies (kJ/mol) for the bonds of the three isomers of methylanisole. Values from this work refer to the different methods of determining BDEs (see main text). Reference values for the analogous bonds in anisole and toluene determined in previous works or from the ATcT database are also reported. In A-Y bonds, A indicates the aromatic ring.

Radical formed bond broken	$xCH_3C_6H_4\dot{O}$ O-CH_3	$x\dot{C}_6H_4OCH_3$ A—CH_3	$xCH_3\dot{C}_6H_4$ A–OCH_3	$x\dot{C}H_2C_6H_4OCH_3$ CH_2—H	$CH_3C_6H_4O\dot{C}H_2$ OCH_2—H	Structure
$oCH_3C_6H_4OCH_3$ (2MA)						
Direct [*this study*]	257.1	425.4	421.9	370.3	402.0	
Pseudo [*this study*]	261.3	429.2	429.0	372.2	401.8	
(exp) [45]	254.8					
(G4) [46]	264.8					
$mCH_3C_6H_4OCH_3$ (3MA)						
Direct [*this study*]	263.2	423.6	420.7	370.6	401.6	
Pseudo [*this study*]	267.4	427.4	427.8	372.5	401.5	
(exp) [45]	263.3					
(G4) [46]	269.4					
$pCH_3C_6H_4OCH_3$ (4MA)						
Direct [*this study*]	257.4	426.3	420.0	368.6	400.9	
Pseudo [*this study*]	261.6	430.1	427.0	370.5	400.8	
(exp) [45]	257.7					
(G4) [46]	264.8					
$C_6H_5OCH_3$						
ATcT [38]	268.6		427.2			
[10]	263.8		419.2		401.7	
[39]	267.4					
$C_6H_5CH_3$						
ATcT [38]		430.5		372.8		
[42]				370.7		

already discussed for anisole [19]. The calculated BDEs for the O–CH_3 bonds for 2 and 4 MA with approximately 257 kJ/mol differ slightly from 3MA (263 kJ/mol) and anisole (264 kJ/mol) [19]. For the other calculated BDEs, differences between the isomers are very low and well within the uncertainty of the applied calculation method (i.e., within 1–2 kJ/mol). The O–CH_3 and A–OCH_3 BDEs in 3MA are in excellent agreement with those of anisole with differences < 0.4 kJ/mol and < 1.5 kJ/mol for those derived with analogous methodologies, respectively. This reveals that the additional methyl substituent in the meta position has almost no impact on the reactivity of the methoxy substituent, as confirmed in other cases for poly-substituted aromatics [12]. Instead, the presence of the methyl group in the ortho and para positions in 2MA and 4MA lowers substantially the BDEs of the methoxy group. Previous works [43–45] analyzed the fundamental reasons behind such substituent effects in anisole and in the corresponding phenoxy-like radicals. Essentially, methyl substituent is an electron donating group that tends to destabilize the aromatic ring with respect to anisole -where the methoxy group is a π-donor- due to a repulsive π-saturation effect. On the contrary, the presence of methyl (the electron donor) enhances the aromatic resonance and stabilizes the phenoxy radical, where the O atom is a π-acceptor, hence its charge and spin density become more negative due to the interactions with the methyl group. In the latter, the polar effect is also enhanced by a spin delocalization effect. Similar to the present results, previous works also found that such polarization effects are less pronounced for substituents in the meta position with respect to those in the ortho and para positions. It is also interesting to compare the absolute values of the energies of 2MA, 3MA and 4MA and the corresponding phenoxy-like radicals (see Table S3). Among the molecules, the hierarchy is 2MA < 3MA < 4MA, with energies of $0 < 1.6 < 4$ kJ/mol with respect to 2MA; among the phenoxy-like radicals instead the hierarchy is 2MA < 4MA < 3MA, with energies of $0 < 4 < 8$ kJ/mol with respect to 2MA. In addition to the effects discussed above, the stability of 2MA and of its radical are probably further enhanced by the electronic interactions between the methyl substituent and the oxygen of the methoxy group.

Due to the high sensitivity of the O–CH_3 bond cleavage on the reactivity of the entire system a relatively small difference in BDE of 6 kJ/mol can lead to a considerable effect on the kinetic model predictions. For this reason, our calculated results have been compared to available data from literature, as shown in Fig. 3. Li et al. [46] also calculated BDEs using G4 methodology and Suryan et al. [45] determined BDEs experimentally. Although the results differ in absolute terms by a maximum of 10 kJ/mol the results confirm the trend that the BDE of 3MA is higher than for 2MA and 4MA.

It is also worth discussing the difference in the BDEs found with the two methodologies adopted, i.e., "direct" and "pseudo" as in Table 2 and Fig. 3. The BDEs obtained with the two methodologies generally agree. However, the extent of the agreement largely depends on the type of broken bond. Results for C–H BDEs agree well within 2 kJ/mol. Instead, the largest discrepancy is observed for the loss of the OCH_3 group (7 kJ/mol), while differences of about 4 kJ/mol are observed for the O–CH_3 and A–CH_3 fissions where A represents the aromatic ring. Larger differences might indicate a larger uncertainty in the estimates of the corresponding BDEs, possibly attributed also to the type of scheme adopted in determining the formation enthalpies for the radical species. In the case of O–CH_3 fission, which is the most sensitive for kinetic modelling, the direct method leads to better agreement with the experimental results of Suryan et al. [47]. However, the uncertainty of these results is not declared in the original reference. Instead, the BDE for 3MA computed from the formation enthalpies (pseudo-exp) is in excellent agreement with the reference values for anisole, which is expected to be almost identical to that of 3MA. For the above reasons, the pseudo-experimental approach was preferred in the determination of BDEs of this work.

Finally, concerning the formation enthalpy of the alkyl-peroxy radical on the methoxy side of 2MA radical ($oCH_3C_6H_4OCH_2O\dot{O}$), the $O_2 + oCH_3C_6H_4OCH_2 = oCH_3C_6H_4OCH_2O\dot{O}$ reaction was considered as reference. The formation enthalpy of $oCH_3C_6H_4OCH_2O\dot{O}$ at 298 K was found to be −51.9 kJ/mol. As the uncertainty of this calculation might be large, a benchmarking with the $O_2 + C_6H_5 = C_6H_5O\dot{O}$ was attempted, as in the latter case reference data from the ATcT database [37] are available. The formation enthalpy computed with this methodology resulted in an overprediction of the reference data by 8.4 kJ/mol, thus indicating a potentially large overestimation also in the case of $oCH_3C_6H_4OCH_2O\dot{O}$. Therefore, we decided to lower the formation enthalpy of $oCH_3C_6H_4OCH_2O\dot{O}$ to −59.9 kJ/mol, which is incidentally also in better agreement with the estimate obtained using group additivity through RMG (−62.8 kJ/mol) and leads to better agreement with the experimentally measured ignition delay times.

3.2.2. Isomerization rate parameters

Rate calculations have been performed for the isomerization between the two 2MA radicals carrying the radical position on the methyl and methoxy side chain. As mentioned before, this reaction is important to properly describe the reactivity of 2MA. Fig. 4 shows the calculated rate parameters at the high-pressure limit for the forward and backward reaction. A table of the pressure dependent rate parameters is provided in the supplemental material (Table S1). It can be seen that the reaction from the radical position on the methoxy side to the radical position on the methyl side is significantly faster due to the higher stability of the product caused by the resonance of the free electron on the methyl group

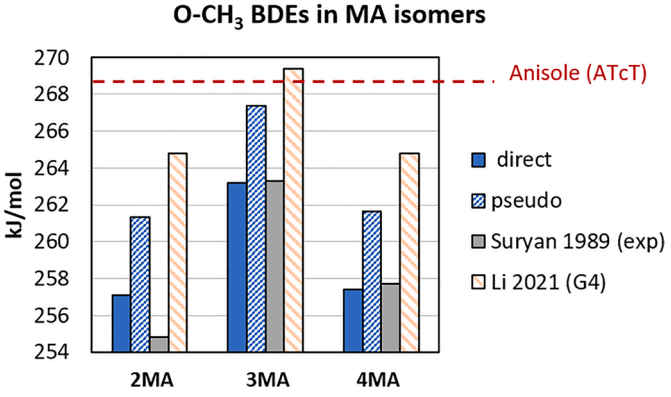

Fig. 3. Comparison of O–CH_3 BDE to literature values of Li et al. [46] and of Suryan et al. [45]. "Direct" refers to BDEs computed from the bond-fission reactions while "pseudo" refers to the values extracted from the formation enthalpies. A dashed line with the reference values obtained for anisole is also reported.

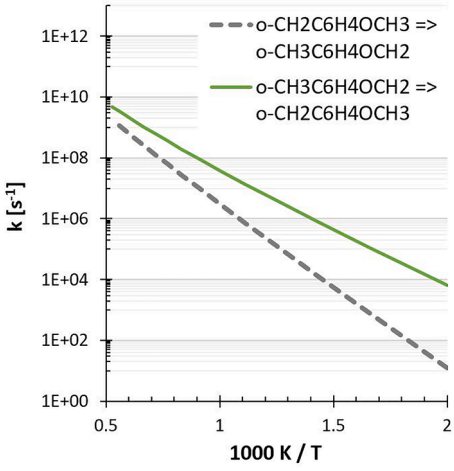

Fig. 4. Calculated rate parameters for the isomerization of 2MA radicals.

with the aromatic ring (i.e., the reaction $oCH_3C_6H_4O\dot{C}H_2$ => $o\dot{C}H_2C_6H_4OCH_3$ is exothermic by 31.8 kJ/mol with a computed energy barrier of 85.4 kJ/mol). However, in absence of competing fast reactions for the consumption of $o\dot{C}H_2C_6H_4OCH_3$, the reverse isomerization reaction $o\dot{C}H_2C_6H_4OCH_3$ => $oCH_3C_6H_4O\dot{C}H_2$ effectively converts the majority of $o\dot{C}H_2C_6H_4OCH_3$ in 2 MA to $oCH_3C_6H_4O\dot{C}H_2$ despite its lower rate. Further discussion of the reaction pathways of the 2MA radicals will be presented in Section 5 using the kinetic model proposed herein.

It is important to note that the discussed isomerization reaction becomes possible due to the vicinity of the two lateral methoxy and methyl groups in 2MA. Similar isomerization for 3MA or 4 MA would have to undergo a multi-step reaction scheme, i.e., OCH_3 H-transfer to the ring, methylene walk, and final transfer to the CH_2 group. Calculations for the initial step of this sequence resulted in barrier heights of about 250 kJ/mol, which is significantly higher than in the case of 2MA. Thus, isomerization between the fuel radicals in the case of 3MA and 4MA are assumed to be irrelevant.

4. Kinetic model development

The kinetic model development was built upon the previously published anisole model [19]. This model was recently extended and optimized to describe the oxidation behaviour of benzyl alcohol in a combined investigation with benzaldehyde and phenol [48]. This model is further expanded in this study by constructing the sub-mechanisms for the three methylanisole isomers 2MA ($oCH_3C_6H_4OCH_3$), 3MA ($mCH_3C_6H_4OCH_3$), and 4MA ($pCH_3C_6H_4OCH_3$).

Thermodynamic properties for all three isomers and their major radicals (excluding only phenyl-like radicals) were computed as described in Section 3 with an estimated uncertainty of ± 1–2 kJ/mol for the molecules and possibly up to 4 kJ/mol for the radicals. An overview of all species, the names used in the mechanism and their corresponding SMILES identifiers can be found in the supplemental material (Table S2). In addition, the thermodynamic properties of the alkyl-peroxy radical on the methoxy side of the 2MA radical ($oCH_3C_6H_4OCH_2O\dot{O}$) has been calculated as discussed above. Thermodynamic data for other species has been estimated using group additivity method implemented in RMG [49].

Apart from the differences in the O–CH_3 bond, the BDE calculations showed no considerable differences in the bond strengths of the three methylanisole isomers, also not compared to anisole or toluene for the respective side groups. Consequently, reaction classes and rate parameters for the MA isomers are taken in direct analogy to anisole [19] for the methoxy side group and to toluene [50] for the methyl side group. For H-atom abstraction reactions by O_2, $\dot{O}H$, $\dot{C}H_3$, and H recently calculated rates have been considered [10]. Thus, reactions on the different side groups are considered to be largely independent from each other and also for subsequent intermediates the same reaction classes and rate parameters as for the corresponding reference compound, either anisole or toluene, are used.

Besides this similar modeling approach for all isomers, two major differences in the sub-models must be noted. First, as already mentioned in Section 3.2.1 the O–CH_3 bond strengths in 2MA and 4MA are about 6 kJ/mol lower compared to anisole. This is considered by lowering the activation energy of the unimolecular decomposition of 2MA and 4MA towards the cresol radical and $\dot{C}H_3$ accordingly. Second, the proximity of the side groups in 2MA allows for additional reactions that are unlikely in 3MA and 4MA and not possible in toluene or anisole. On the one hand, the isomerization reaction between the two side groups in 2MA (see Section 3.2.2) and, on the other hand, low-temperature pathways that become possible for 2MA as the isomerization from $R\dot{O}_2$ ($\dot{O}OCH_2$–C_6H_4–OCH_3) to $\dot{Q}OOH$ ($HOOCH_2$–C_6H_4–$O\dot{C}H_2$) can be expected to be considerably fast. As a first estimate, rate parameters for the $R\dot{O}_2$ to $\dot{Q}OOH$ isomerization and the subsequent formation of the cyclic ether are taken in analogy to n-pentane (1,7p and ε-$\dot{Q}OOH$ [51]). An alternative to this rough estimation could be an analogy to o-xylene, since similarly to 2MA two side groups are in close vicinity to each other and attached to an aromatic ring. A comparison to the rate parameters in o-xylene low temperature oxidation [14] revealed similar values for the cyclic ether formation but 60 times higher rate coefficients for the $R\dot{O}_2$ to $\dot{Q}OOH$ isomerization. Using such high rate parameters lead to an overprediction of the reactivity at low temperatures of about a factor of 5 at 850 K (see Fig. S1). Thus, using a direct analogy to xylene for rate estimation was avoided. Future work on this reaction system would be necessary to optimize the model in this respect. For consistency, also the second addition to O_2 and subsequent reactions have been defined in analogy to n-pentane.

For all isomers, cresol radicals are formed in significant amounts by the unimolecular decomposition via O–CH_3 bond breaking. As a consequence, the fate of the cresol radical has an important impact on the reactivity of the system (see Section 5.3) and a few updates have been introduced to the cresol sub-model. First, reactions that were not considered in the original base mechanism were adopted from the CRECK mechanism. Second, the reaction of the cresol radical with $H\dot{O}_2$ forming $\dot{O}CH_3C_6H_4O + \dot{O}H$ was estimated in analogy to $C_6H_5\dot{O} + H\dot{O}_2$ <=> $\dot{O}C_6H_5O + \dot{O}H$ [52]. Third, a pressure dependent rate expression for the decomposition reaction of cresol to cresoxy and a hydrogen radical ($HOC_6H_4CH_3$ <=> $\dot{O}C_6H_4CH_3 + \dot{H}$) has been adopted from [50].

Finally, tuning of a few rate parameters was necessary to achieve better agreement between the kinetic model predictions and the experimental results. Initial simulations overpredicted the reactivity of 3MA and 4MA at low temperatures. For this reason, the rate constants of the reaction classes RH + $R\dot{O}_2$ and $H\dot{O}_2$ + $R\dot{O}_2$ were decreased by a factor of 2 and the H-atom abstraction by molecular oxygen on the methyl side was increased by a factor of 3 as its reverse reaction was inhibiting reactivity. Based on the current limited knowledge specific to oxygenated aromatic hydrocarbons, and of methyl anisole isomers in particular, at intermediate and low temperature oxidation conditions and considering the preliminary and interpretative nature of the current model we believe that the rate modifications described here are moderate and within the expected uncertainty of the rate parameter estimations.

The resulting models in CANTERA format are provided as supplemental material. All references and rate coefficient modifications are added as comments in the mechanism file next to the corresponding reaction rate parameters for easier reference. In addition, uncommented mechanisms in CHEMKIN format are also provided.

5. Results

5.1. Ignition delay times

Fig. 5 presents the ignition delay times measured in ST and RCM against predictions using the model developed in this study. IDT show the expected Arrhenius behavior as a function of inverse temperature. Moreover, as expected IDT decrease with increasing pressure. 3MA and 4MA show very similar ignition delay times in the entire temperature regime, while for 2MA significantly shorter ignition delay times are observed.

The kinetic model is able to describe the main trends and the relative reactivity of the three isomers, but deviates from the measurements in some cases outside the uncertainty limits. In fact, at high temperatures and low pressures, the model tends to underpredict the reactivity of 2MA by 50 %. Moreover, between 3MA and 4MA the model predicts maximum differences in ignition delay times of about 30 % at 10 bar, which are not visible in the experimental results. Finally, in the RCM regime the ignition delay of 4MA is slightly overpredicted by about 45 % at 10 bar and low temperatures, whereas the ignition delay of 3MA is underpredicted by approximately 40 % at 20 bar and higher temperatures.

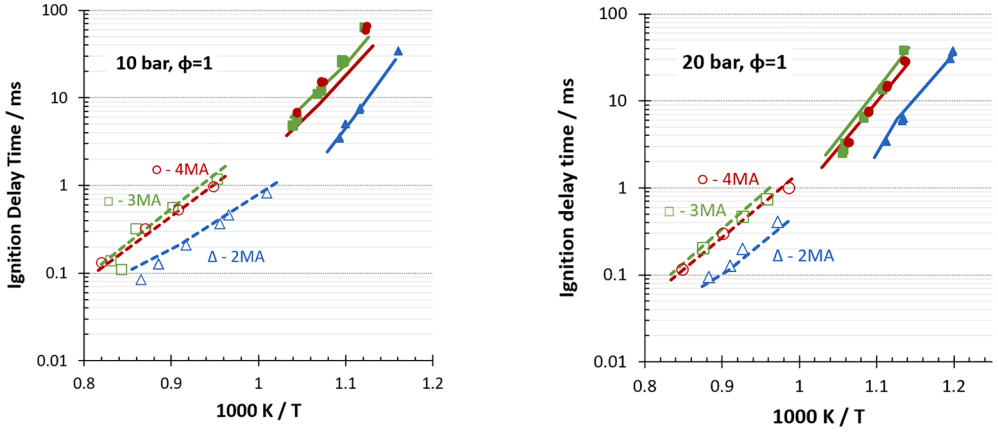

Fig. 5. Measured and predicted Ignition Delay Times (IDT) for stoichiometric conditions and air-like dilution. Open symbols and dashed lines: ST regime. Closed symbols and solid lines: RCM regime.

While in experiment only pressure and temperature variations were performed, additional simulations using the developed kinetic model of this study allow to evaluate the effect of changing the equivalence ratio (see Fig. S3). As expected, the reactivity decreases with decreasing equivalence ratio within the investigated regime of conditions (20 bar, 800–1250 K, φ = 0.5 – 2.0). However, the differences in reactivity between the three isomers remain about the same.

5.2. Rate of production analysis (ROP)

As the kinetic model is able to represent the major aspects of the ignition behavior of all three isomers results from kinetic analyses are used to discuss and highlight the main features of the undergoing chemistry specifically focusing on the differences between the three fuels. For this purpose, a rate of production (ROP) analysis is performed at 20 bar and two temperatures representing the high and low temperature ignition regime (900 K and 1100 K) corresponding to 20 % of the fuel consumption (Fig. 6).

Consistently, all three isomers are mainly consumed by H-atom abstraction and unimolecular decomposition reactions. Abstractions from the methyl group are slightly faster than those from the methoxy group and in both cases the abstraction by ȮH dominates. At lower temperatures the H-atom abstractions dominate the fuel consumption whereas at higher temperatures the bond-fission reactions gain

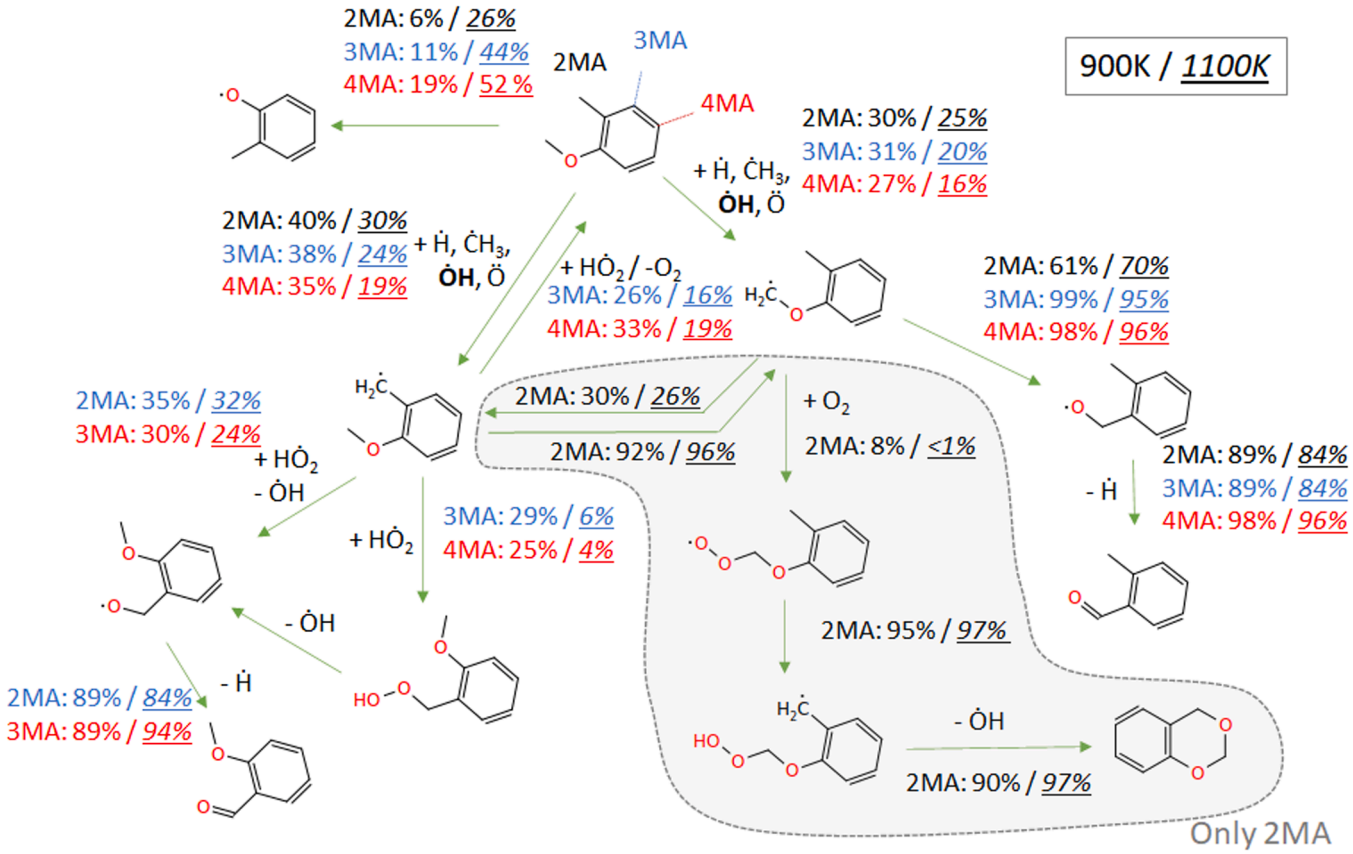

Fig. 6. Major reaction pathways at the time when 20 % of the fuel is consumed, 20 bar, φ=1. For simplicity, only structures for 2MA are shown. Underlined italic numbers represent fluxes at 1100 K, other numbers the fluxes for 900 K. Fluxes for different MA isomers are indicated by 2MA, 3MA, and 4MA, respectively.

importance as can be expected. Nevertheless, the unimolecular decomposition involving the O–CH_3 bond breaking on the methoxy side plays a considerable role even at low temperatures due to its low barrier [19].

Besides these similarities, major differences between 2MA and the other two isomers can be observed. As discussed in Section 3.2.2, the vicinity of the two functional groups in 2MA allows for isomerization between the radicals and low temperature reactions. For the benzyl-like 2MA radical ($oC\dot{H}_2C_6H_4OCH_3$) potentially competing reactions, particularly reactions with $H\dot{O}_2$, are comparably slow so that the majority of this radical is consumed via isomerization to the 2MA anisyl-like radical ($oCH_3C_6H_4O\dot{C}H_2$). This radical can be converted to $oCH_3C_6H_4CH_2\dot{O}$ via a cyclic transition state [19], such that the isomerization back to $oC\dot{H}_2C_6H_4OCH_3$ becomes less important despite the faster unimolecular rate constant of the backward isomerization. In essence, the concentration of the anisyl-like radical is on average 40 times smaller at 900 K and 22 times smaller at 1100 K due to its consumption to $oCH_3C_6H_4CH_2\dot{O}$ and subsequent β-scission. At low temperatures, also the addition of $oCH_3C_6H_4O\dot{C}H_2$ to molecular oxygen becomes competitive with the isomerization reactions forming the corresponding alkylperoxy ($R\dot{O}_2$) radical. Subsequently, the alkylperoxy radical mainly isomerizes by H-migration from the methyl group to form the corresponding $\dot{Q}OOH$ which reacts further to form a cyclic ether and an $\dot{O}H$ radical. This relatively fast low temperature pathway is therefore able to enhance the formation of reactive radicals which leads to higher fluxes into the H-atom abstraction channels and ultimately also to a higher reactivity of 2MA in comparison to 3MA or 4MA, where this pathway is not available. As the isomerization and fast low temperature pathways are not possible for 3MA and 4MA, the corresponding $CH_3C_6H_4O\dot{C}H_2$ radicals react almost exclusively via the fast isomerization to $CH_3C_6H_4CH_2\dot{O}$, which is converted to the corresponding aldehyde losing an $\dot{H}$ atom. The aldehyde is then consumed (not shown in Fig. 6) by H-atom abstractions on the aldehydic side group followed by a rapid decomposition forming carbon monoxide and the methyl phenyl radical. Additionally, in the case of 3MA and 4MA the stable benzyl-like $\dot{C}H_2C_6H_4OCH_3$ radicals are consumed mainly via reactions with $H\dot{O}_2$. The addition of $H\dot{O}_2$ to this radical followed by the O–O bond breaking and alternatively the direct route to $\dot{O}CH_2C_6H_4OCH_3$ convert $H\dot{O}_2$ radicals to more reactive $\dot{O}H$ radicals and are therefore reactivity enhancing (Section 5.3). Furthermore, the β-scission of the resulting $\dot{O}CH_2C_6H_4OCH_3$ also releases an $\dot{H}$ atom, which further increases the reactivity of the system. In contrast, the reaction of the fuel radical with $H\dot{O}_2$ can also lead to the formation of molecular oxygen and the fuel (reverse H-abstraction reaction by O_2), which substantially reduces the reactivity as it forms two stable species.

The competition on $H\dot{O}_2$ radicals has also important implications on the consumption of the cresol radical. At lower temperatures, the consumption of the cresol radical is dominated by reaction with $H\dot{O}_2$ either forming cresol and O_2 or $\dot{O}CH_3C_6H_4O$ and $\dot{O}H$. The latter reaction is one of the major pathways for the formation of $\dot{O}H$ (the major responsible for fuel consumption through H-atom abstraction) together with the decomposition of hydrogen peroxide ($H_2O_2 + M = \dot{O}H + \dot{O}H + M$), dominantly formed via $H\dot{O}_2 + H\dot{O}_2 = H_2\dot{O}_2 + O_2$. In the case of 2MA, the reaction of the phenyl-like radical with $H\dot{O}_2$ back to the fuel and O_2 is not of relevance and thus a higher concentration of $H\dot{O}_2$ radicals is available in the system. In fact, at 900 K $H\dot{O}_2$ concentration is about 5 times higher in the case of 2MA compared to 4MA (see Fig. S2). Overall, the higher amount of $H\dot{O}_2$ radicals fosters $\dot{O}H$ production, which explains the increased importance of the H-atom abstraction reactions versus the O–CH_3 bond-fission reaction in the case of 2MA compared to 3MA or 4MA. At high temperatures unimolecular consumption reactions of the cresol radical gain importance as can be expected.

Finally, slight differences in the fluxes exist also between 3MA and 4MA, particularly in the bond-fission reaction pathway. These differences mainly stem from the lower barrier of the O–CH_3 bond breaking in 4MA, as discussed in Section 3.2.1. In contrast to 2MA where, due to the vicinity of the side groups, alternative reaction pathways become possible which led to higher fluxes into the H-atom abstraction pathways, for 3MA and 4MA the reaction scheme is very similar. Thus, the increased flux into the unimolecular decomposition directly leads to a slightly higher reactivity of 4MA in simulation compared to 3MA. Clear evidences of such limited difference, however, are not highlighted by the current experimental measurements as the IDT of 3MA and 4MA agree within experimental uncertainty.

5.3. Sensitivity analysis

For further analysis and for identifying the reactions controlling reactivity, brute force sensitivity analyses to rate parameters on ignition delay times were performed. For this purpose, the A-factor of each reaction was increased by a factor of 2 and its effect on the ignition delay time expressed by the sensitivity parameter $S = (IDT\text{-}IDT_{Ref})/IDT_{Ref}$, where IDT describes the ignition delay time prediction with A-factor variation and IDT_{ref} the original IDT prediction. Thus, S describes the percentual change of ignition delay time due to an A-factor variation and negative values of S indicate a reactivity enhancing effect while positive values indicate a reactivity inhibiting effect. Consistent to the pathway analysis, also the sensitivity analyses were performed at 20 bar, φ=1.0 and two temperatures (900 K and 1100 K) and its results are shown in Fig. 7. Additional results for varying pressure and equivalence ratios are provided in the Supplemental Material (Fig. S4–6). Overall, these sensitivities show the same trends as in Fig. 7 and vary only slightly within the investigated parameter range ($\varphi = 0.5 - 2.0$, $p = 10\text{-}40$ bar).

Overall, the sensitivity analyses show consistent trends compared to the pathway analysis. For all MA isomers, the bond fission to the cresol radical ($\dot{O}C_6H_4CH_3$) and methyl plays an important role even at low temperatures due to the weak O–CH_3 bond. As a consequence, also the subsequent reactions of the cresol radical are decisive for the overall reactivity of all isomers. The most important pathway appears to be the backward H-atom abstraction reaction with O_2, which strongly inhibits reactivity as it converts two radicals into two stable species. In contrast, the cresol radical can also react with $H\dot{O}_2$ towards $\dot{O}CH_3C_6H_4O + \dot{O}H$ (analogy to $C_6H_5\dot{O} + H\dot{O}_2 = o\text{-}OC_6H_4\dot{O} + \dot{O}H$) which is reactivity enhancing as this pathway produces highly reactive $\dot{O}H$ radicals. Finally, also the radical recombination of the cresol radical and $\dot{H}$ forming cresol has an important inhibiting effect especially at higher temperatures, as it proceeds in the direction of the recombination and therefore reduces the concentration of radicals in the system.

Major differences in the sensitivities between the MA isomers can be observed in agreement to the different dominant reaction pathways discussed in Section 5.2 (cf. Fig. 6). 2MA reacts mainly via $oCH_3C_6H_4O\dot{C}H_2$ and $oCH_3C_6H_4CH_2\dot{O}$ towards 2-methylbenzaldehyde ($o\text{-}CH_3C_6H_4CHO$). For this reason, the consumption of the aldehydic species by $\dot{O}H$ and $\dot{O}$ influences significantly the overall reactivity. Alternatively, $oCH_3C_6H_4O\dot{C}H_2$ can undergo addition to molecular oxygen. It should be noted that the reaction $\dot{R} + \dot{O}_2 = R\dot{O}_2$ is not highly dependent on the absolute value of the rate parameter but more on the equilibrium between forward and reverse rate and thus does not show up in the sensitivity analysis. However, it is critical for the low temperature pathway which potentially produces a large number of $\dot{O}H$ radicals and competes with the isomerization of $oCH_3C_6H_4O\dot{C}H_2$ towards $oCH_3C_6H_4CH_2\dot{O}$. For this reason, this latter appears as reactivity inhibiting. The isomerization from the alkylperoxyl radical ($oCH_3C_6H_4OCH_2O\dot{O}$) to the alkylhydroperoxide ($o\text{-}\dot{C}H_2C_6H_4OCH_2OOH$) is the subsequent step to the addition of the fuel radical to O_2 in the low temperature pathway towards $\dot{O}H$ formation and is therefore reactivity enhancing.

It is interesting to note that, in the case of 2MA, no H-atom abstractions from the fuel rank amongst the 10 most sensitive reactions and no other primary reactions apart from the methoxy bond-fission

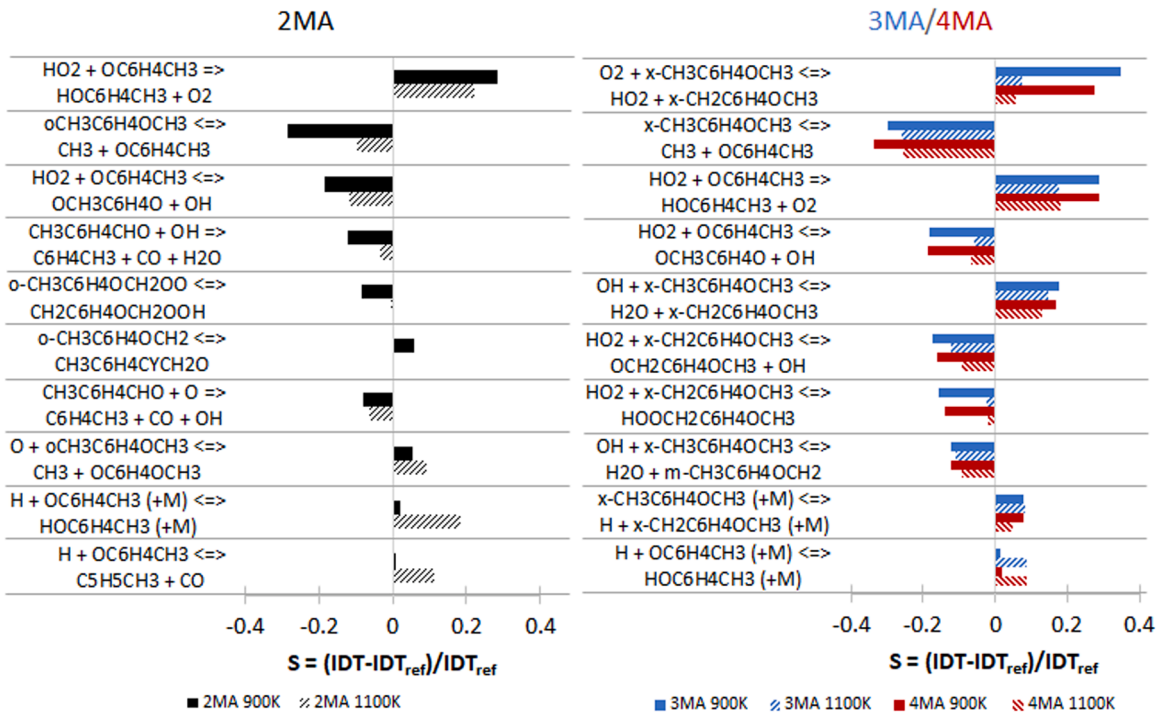

Fig. 7. Sensitivity analysis of ignition delay times to rate constants at 20 bar, φ=1. Positive values for S indicate reactivity suppressing reactions, negative values reactivity enhancing reactions. Only the 10 most sensitive and fuel specific reactions are shown.

control the reactivity of 2MA. Instead, in the case of 3MA and 4MA the H-atom abstraction by ȮH from both side groups plays a considerable role. Furthermore, as the benzyl-like radical cannot isomerize to the anisyl-like radical, bimolecular reactions consuming $\dot{C}H_2C_6H_4OCH_3$ become important. Thereby the reaction pathways producing ȮH via reaction of the fuel radical with $H\dot{O}_2$ are reactivity-enhancing as they convert a relatively low reactive radical into a high reactive radical.

5.4. Discussion on uncertainties of the kinetic model

As shown in Section 5.1 the model is able to describe the global fuel reactivity reasonably well. However, it is important to note that considerable uncertainties in the current model exist that need further attention in future work. These are highlighted in the following aiming to guide and motive ongoing and future studies on these fuels.

(I) According to the BDE analysis presented in Section 3.2.1, no substantial differences between the methylanisole isomers and the respective mono-substituted aromatics (toluene, anisole) exist with the exception of O–CH_3 bond-fission in 2MA and 4MA. Hence, direct analogies to anisole and toluene were considered suitable for estimating rate parameters. Anisole and particularly toluene have been studied in detail previously so that reliable rate parameters can be expected. However, this aspect was verified through the BDE analogies only for the reactions directly involving the fuel but not for all intermediates with different functional groups. The sensitivity analysis (Fig. 7) shows a high sensitivity to cresol related intermediates which is not a well-studied component. Furthermore, the model does not distinguish between ortho, meta, and para configuration of cresol and its radical. Thus, more investigation on cresol would be required to confirm the current mechanism.

(II) Other important intermediates are methylbenzaldehydes (Figs. 6 and 7). Prior work on benzaldehyde [53–55] provide a good basis for the reaction on the aldehydic side group so that on these species no high uncertainties are expected. It is assumed that the reactions from the aldehydic side chain dominate the consumption of the methylbenzaldehydes and consequently no differentiation between ortho, meta, and para configuration is considered in the kinetic model. This approach requires confirmation by further studies directly focusing on such intermediates.

(III) For 2MA, low temperature pathways initiated by the fuel radical addition to O_2 were found to be relevant. Especially the $\dot{R}O_2 = \dot{Q}OOH$ isomerization appears as sensitive (Fig. 7). Currently, rate parameters for this reaction are estimated by analogy to n-pentane which is structurally very different from 2MA, in particular with regards to the different steric hindrance. However, rate parameter estimation in direct analogy to o-xylene lead to a strong overestimation in the reactivity at low temperatures. In any case, the flux into the low temperature pathways is still small under the investigated conditions and further studies under either higher pressures or in mixtures with a radical donor (e.g., dimethyl ether) might allow experimental investigations at lower temperatures to enhance the flux of these pathways. This would increase the sensitivity of these reactions and could ultimately help to further constraining rate coefficients for the associated reactions classes.

6. Conclusions

The current study presents, for the first time, ignition delay times of the three methylanisole isomers measured in a shock tube and a rapid compression machine at 10 and 20 bar for stoichiometric fuel/air mixtures. By using the two experimental facilities a wide regime of temperatures ranging from 880 K to 1220 K was covered. All isomers show Arrhenius-like ignition behaviour, but with a significant higher reactivity of 2MA (i.e., the ortho isomer) over the entire temperature range compared to the other two isomers.

In addition to the experimental investigation, a kinetic model was developed to analyse the oxidation pathways of the methylanisole isomers. Comparison of calculated BDEs to the monosubstituted aromatics toluene and anisole suggests that direct analogies to these compounds

for estimating rate parameters of the methylanisole isomers, with the exception of the bond-fission of the O–CH_3 bond that requires smaller activation for the ortho and para isomers. The resulting model is capable of describing the experimentally observed ignition behaviour well. Rate of production and sensitivity analyses using the developed model reveal that the observed differences between the ignition behaviour of 2-methylanisole versus 3- and 4-methylanisole mainly stem from isomerization reactions between the fuel radicals on the side groups and low temperature pathways, both becoming possible due to the vicinity of the side groups in the ortho configuration. However, uncertainties in the cresol sub-mechanism, which influences the ignition behaviour of all three isomers due to the dominance of the unimolecular decomposition via O–CH_3 bond-breaking on the methoxy side, requires further attention in future studies to confirm rate parameters assigned in the current model. Furthermore, rate parameters for the low temperature pathways in 2-methylanisole are derived by relatively rough analogies to n-pentane due to lacking information on comparable systems.

CRediT authorship contribution statement

Karl Alexander Heufer: Writing – original draft, Supervision, Project administration, Investigation, Funding acquisition, Formal analysis, Conceptualization. **Rene Daniel Büttgen:** Validation, Investigation. **Luna Pratali Maffei:** Writing – original draft, Validation, Software, Investigation, Formal analysis. **Matteo Pelucchi:** Writing – review & editing, Supervision, Project administration, Conceptualization.

Declaration of competing interest

The authors declare that they have no known competing financial interests or personal relationships that could have appeared to influence the work reported in this paper.

Acknowledgement

The authors at RWTH Aachen University gratefully acknowledge the German Research Foundation (DFG) for financial support provided for this research (Project 290644284).

L.P.M. work was carried out within the NEST - Network 4 Energy Sustainable Transition (D.D. 1561 of 11/10/2022, PE0000021). This manuscript reflects only the authors' views and opinions, neither the European Union nor the European Commission can be considered responsible for them.

Supplementary materials

Supplementary material associated with this article can be found, in the online version, at doi:10.1016/j.combustflame.2024.113533.

References

[1] D. Gschwend, P. Soltic, A. Wokaun, F. Vogel, Review and performance evaluation of fifty alternative liquid fuels for spark-ignition engines, Energy Fuel 33 (2019) 2186–2196.
[2] D. Gschwend, S. Müller, A. Wokaun, F. Vogel, Optimum fuel for spark ignition engines from lignin pyrolysis oil, Energy Fuel 32 (2018) 9388–9398.
[3] F. Battin-Leclerc, N. Delort, I. Meziane, O. Herbinet, Y. Sang, Y. Li, Possible use as biofuels of monoaromatic oxygenates produced by lignin catalytic conversion: a review, Catal. Today. 408 (2023) 150–167.
[4] P. Zhang, N.W. Yee, S.V. Filip, C.E. Hetrick, B. Yang, W.H. Green, Modeling study of the anti-knock tendency of substituted phenols as additives: an application of the reaction mechanism generator (RMG), Phys. Chem. Chem. Phys 20 (2018) 637–649.
[5] R.L. McCormick, M.A. Ratcliff, E. Christensen, L. Fouts, J. Luecke, G.M. Chupka, J. Yanowitz, M. Tian, M. Boot, Properties of oxygenates found in upgraded biomass pyrolysis oil as components of spark and compression ignition engine fuels, Energy Fuel 29 (2015) 2453–2461.
[6] M. Tian, R.L. McCormick, M.A. Ratcliff, J. Luecke, J. Yanowitz, P.A. Glaude, M. Cuijpers, M.D. Boot, Performance of lignin derived compounds as octane boosters, Fuel 189 (2017) 284–292.
[7] J. Yanowitz, M.A. Ratcliff, R.L. McCormick, J.D. Taylor, M.J. Murphy, Technical Report, NREL/TP-5400-67585, NREL, United States, 2017.
[8] R. Xu, T. Ye, X. Yue, Z. Yang, W. Yu, Y. Zhang, M. Bell, L. Morawska, P. Yu, Y. Zhang, Y. Wu, Y. Liu, F. Johnston, Y. Lei, M.J. Abramson, Y. Guo, S. Li, Global population exposure to landscape fire air pollution from 2000 to 2019, Nature 621 (2023) 521–529.
[9] L. Pratali Maffei, M. Pelucchi, T. Faravelli, C. Cavallotti, Theoretical study of sensitive reactions in phenol decomposition, React. Chem. Eng. 5 (2020) 452–472.
[10] L. Pratali Maffei, M. Pelucchi, R.D. Büttgen, K.A. Heufer, T. Faravelli, C. Cavalotti, Rate constants for H-atom abstraction reactions from mono-aromatic hydrocarbons by H, CH3, OH and 3O2: a systematic theoretical investigation, Combust. Flame (2022) 112421.
[11] M. Pelucchi, C. Cavallott, A. Cuoci, T. Faravelli, A. Frassoldati, E. Ranzi, Detailed kinetics of substituted phenolic species in pyrolysis bio-oils, React. Chem. Eng. 4 (2019) 490–506.
[12] L. Pratali Maffei, T. Faravelli, C. Cavallotti, M. Pelucchi, Electronic structure-based rate rules for Ḣ ipso addition–elimination reactions on mono-aromatic hydrocarbons with single and double OH/CH3/OCH3/CHO/C2H5 substituents: a systematic theoretical investigation, Phys. Chem. Chem. Phys. 22 (2020) 20368–20387.
[13] H.P.S. Shen, M.A. Oehlschlaeger, The autoignition of C8H10 aromatics at moderate temperatures and elevated pressures, Combust. Flame. 156 (2009) 1053–1062.
[14] I. Meziane, N. Delort, O. Herbinet, R. Bounaceur, F. Battin-Leclerc, A comparative study of the oxidation of toluene and the three isomers of xylene, Combust. Flame 257 (2023) 113046.
[15] N. Delort, I. Meziane, M. Framinet, R. Bounaceur, J. Bourgalais, F. Battin-Leclerc, O. Herbinet, An experimental and modeling investigation of the combustion of anisole and guaiacol, Fuel 362 (2024) 130832.
[16] I. Meziane, N. Delort, J. Bourgalais, et al., First experimental study of the low-temperature oxidation of the three isomers of cresol, Proc. Eur. Combust. Meet. (2023).
[17] A.M. Verma, N. Kishore, Molecular modelling approach to elucidate the thermal decomposition routes of vanillin, New J. Chem. 41 (2017) 8845.
[18] M. Nowakowska, O. Herbinet, A. Dufour, P.A. Glaude, Kinetic study of the pyrolysis and oxidation of guaiacol, J. Phys. Chem. A. 122 (2018) 7894–7909.
[19] R.D. Büttgen, M. Tian, Y. Fenard, H. Minwegen, M.D. Boot, K.A. Heufer, An experimental, theoretical and kinetic modelling study on the reactivity of a lignin model compound anisole under engine-relevant conditions, Fuel 269 (2020) 117190.
[20] R.D. Büttgen, T. Raffius, G. Grünefeld, H.J. Koß, K.A. Heufer, High-speed imaging of the ignition of ethanol at engine relevant conditions in a rapid compression machine, Proc. Comb. Inst. 37 (2019) 1471–1478.
[21] C. Lee, S. Vranckx, K.A. Heufer, S.V. Khomik, Y. Uygun, H. Olivier, R.X. Fernandes, On the chemical kinetics of ethanol oxidation: shock tube, rapid compression machine and detailed modeling study, Z. Phys. Chem. 226 (2012) 1–27.
[22] A. Ramalingam, K. Zhang, A. Dhongde, L. Virnich, H. Sankhla, H.J. Curran, K. A. Heufer, An RCM experimental and modeling study on CH4 and CH4/C2H6 oxidation at pressures up to 160bar, Fuel 206 (2017) 325–333.
[23] G. Mittal, M.P. Raju, C.J. Sung, Vortex formation in a rapid compression machine: influence of physical and operating parameters, Fuel 94 (2012) 409–417.
[24] B.W. Weber, C.J. Sung, M.W. Renfro, On the uncertainty of temperature estimation in a rapid compression machine, Combust. Flame 162 (2015) 2518–2528.
[25] S.S. Goldsborough, S. Hochgreb, G. Vanhove, M.S. Wooldridge, H.J. Curran, C. J. Sung, Advances in rapid compression machine studies of low- and intermediate-temperature autoignition phenomena, Prog. Energy. Combust. Sci. 63 (2017) 1–78.
[26] K. Zhang, C. Banyon, J. Bugler, H.J. Curran, A. Rodriguez, O. Herbinet, F. Battin-Leclerc, C. B'Chir, K.A. Heufer, An updated experimental and kinetic modeling study of n-heptane oxidation, Combust, Flame 172 (2016) 116–135.
[27] H. Minwegen, U. Burke, K.A. Heufer, An experimental and theoretical comparison of C3–C5 linear ketones, Proc. Comb. Inst. 36 (2017) 561–568.
[28] E.L. Petersen, R.K. Hanson, Nonideal effects behind reflected shock waves in a high-pressure shock tube, Shock Waves 10 (2001) 405–420.
[29] C. Cavallotti, M. Pelucchi, Y. Georgievskii, S.J. Klippenstein, EStokTP: electronic structure to temperature-and pressure-dependent rate constants-a code for automatically predicting the thermal kinetics of reactions, J. Chem. Theory Comput. 15 (2019) 1122–1145.
[30] M. Frisch, G.W. Trucks, H.B. Schlegel, et al., Gaussian 09, revision D. 01, (2009).
[31] H.J. Werner, P.J. Knowles, G. Knizia, F.R. Manby, M. Schütz, Molpro: a general-purpose quantum chemistry program package, WIREs Comput. Mol. Sci. 2 (2012) 242–253.
[32] Y. Georgievskii, J.A. Miller, M.P. Burke, S.J. Klippenstein, Reformulation and solution of the master equation for multiple-well chemical reactions, J. Phys. Chem. A. 117 (2013) 12146–12154.
[33] Da Chai, M. Head-Gordon, Long-range corrected double-hybrid density functionals, J. Chem. Phys. 131 (2009) 174105.
[34] M. Urban, J. Noga, S.J. Cole, R.J. Bartlett, Towards a full CCSDT model for electron correlation, J. Chem. Phys. 83 (1985) 4041–4046.
[35] J.M.L. Martin, Ab initio total atomization energies of small molecules — Towards the basis set limit, Chem. Phys. Lett. 259 (1996) 669–678.
[36] C. Eckart, The penetration of a potential barrier by electrons, Phys. Rev. 35 (1930) 1303–1309.

[37] S.N. Elliott, K.B. Moore, A.V. Copan, et al., Automated theoretical chemical kinetics: predicting the kinetics for the initial stages of pyrolysis, Proc. Combust. Inst. 38 (2021) 375–384.
[38] B. Ruscic, D.H. Bross, Active Thermochemical Tables (ATcT) Values Based On ver. 1.122d of the Thermochemical, Network Argonne National Laboratory, 2018.
[39] L. Pratali Maffei, A.D. Libera, T. Faravelli, C. Cavallotti, Theoretical and kinetic analysis of anisole and cresol primary reactivity in pyrolysis and oxidation, PROCI (2024) submitted.
[40] J.L. Hales, E.B. Lees, D.J. Ruxton, Thermodynamic properties of organic oxygen compounds. Part 18.—Vapour heat capacities and heats of vaporization of ethyl ketone, ethyl propyl ketone, methyl isopropy1 ketone, and methyl phenyl ether, Trans. Faraday Soc. 63 (1967) 1876–1879.
[41] D.C. Tardy, B.S. Rabinovitch, Collisional energy transfer. Thermal unimolecular systems in the low-pressure region, J. Chem. Phys. 45 (1966) 3720–3730.
[42] M. Pelucchi, C. Cavallotti, T. Faravelli, S.J. Klippenstein, H-Abstraction reactions by OH, HO2, O, O2 and benzyl radical addition to O2 and their implications for kinetic modelling of toluene oxidation, Phys. Chem. Chem. Phys. 20 (2018) 10607–10627.
[43] Y.D. Wu, D.K.W. Lai, A density functional study of substituent effects on the O-H and O-CH3 bond dissociation energies in phenol and anisole, J. Org. Chem. 61 (1996) 7904–7910.
[44] C. Hansch, A. Leo, R.W. Taft, A survey of hammett substituent constants and resonance and field parameters, Chem. Rev. 91 (1991) 165–195.
[45] M.M. Suryan, S.A. Kafafi, S.E. Stein, Dissociation of substituted anisoles: substituent effects on bond strengths, J. Am. Chem. Soc. 111 (1989) 4594–4600.
[46] R. Li, T. Du, J. Liu, A.J.A. Aquino, J. Zhang, Theoretical study of O-CH3 bond dissociation enthalpy in anisole systems, ACS. Omega 6 (2021) 21952–21959.
[47] M.M. Suryan, S.A. Kafafi, S.E. Stein, The thermal decomposition of hydroxy- and methoxy-substituted anisoles, J. Am. Chem. Soc. 111 (1989) 1423–1429.
[48] K.A. Heufer, R.D. Büttgen, L. Pratali Maffei, M. Pelucchi, Auto-ignition characteristics of oxygenated aromatic compounds: benzyl alcohol, benzaldehyde, and phenol, PROCI (2024) submitted.
[49] M.S. Johnson, X. Dong, A. Grinberg Dana, Y. Chung, D. Farina, R.J. Gillis, M. Liu, N.W. Yee, K. Blondal, E. Mazeau, C.A. Grambow, A.M. Payne, K.A. Spiekermann, H.W. Pang, C. Goldsmith, R.H. West, W.H. Green, RMG database for chemical property prediction, J. Chem. Inf. Model. 62 (2022) 4906–4915.
[50] L. Pratali Maffei, M. Pelucchi, T. Faravelli, C. Cavallotti, Theoretical kinetics of HO2+C5H5: a missing piece in cyclopentadienyl radical oxidation reactions, Proc. Combust. Inst. 39 (2023) 695–703.
[51] J. Bugler, K.P. Somers, E.J. Silke, H.J. Curran, Revisiting the kinetics and thermodynamics of the low-temperature oxidation pathways of alkanes: a case study of the three pentane isomers, J. Phys. Chem. A 119 (28) (2015) 7510–7527.
[52] Y. Wu, S. Panigrahy, A.B. Sahu, C. Bariki, J. Liang, A. Mohamed, S. Dong, C. Tang, H. Pitsch, Z. Huang, H.J. Curran, Understanding the antagonistic effect of methanol as a component in surrogate fuel models: a case study of methanol/n-heptane mixtures, Combust. Flame 226 (2021) 229–242.
[53] S. Namysl, M. Pelucchi, L.P. Maffei, O. Herbinet, A. Stagni, T. Faravelli, F. Battin-Leclerc, Experimental and modeling study of benzaldehyde oxidation, Combust. Flame 211 (2020) 124–132.
[54] J.T. Chen, D. Yu, W. Li, W.Y. Chen, S.B. Song, C. Xie, J.Z. Yang, Z.Y. Tian, Oxidation study of benzaldehyde with synchrotron photoionization and molecular beam mass spectrometry, Combust. Flame 220 (2020) 455–467.
[55] H. Zhao, Y. Zhang, Q. Zhao, Y. Li, Z. Huang, A theoretical study of H-abstractions of benzaldehyde by H, O3 (P), 3O2, OH, HO2, and CH3 radicals: Ab initio rate coefficients and their uncertainty quantification, J. Phys. Chem. A 126 (2022) 7523–7533.